ELSEVIER

Contents lists available at ScienceDirect

Biosensors and Bioelectronics

journal homepage: www.elsevier.com/locate/bios





Development of highly sensitive, flexible dual L-glutamate and GABA microsensors for *in vivo* brain sensing

Sung Sik Chu ^a, Hung Anh Nguyen ^b, Derrick Lin ^c, Mehwish Bhatti ^d, Carolyn E. Jones-Tinsley ^e, An Hong Do ^c, Ron D. Frostig ^{a,d}, Zoran Nenadic ^a, Xiangmin Xu ^{a,f,g}, Miranda M. Lim ^e, Hung Cao ^{a,b,g,h,*}

- ^a Department of Biomedical Engineering, University of California Irvine, CA, 92697, USA
- ^b Department of Electrical Engineering and Computer Sciences, University of California Irvine, 92697, CA, USA
- ^c Department of Neurology, University of California Irvine, CA, 92697, USA
- ^d Department of Neurobiology and Behavior, University of California, CA, 92697, USA
- ^e VA Portland Health Care System, Department of Neurology, Oregon Health and Science University, OR, 97239, USA
- f Department of Anatomy and Neurobiology, University of California Irvine, CA, 92697, USA
- g Center for Neural Circuit Mapping, University of California Irvine, CA, 92697, USA
- ^h Department of Computer Science, University of California Irvine, CA, 92697, USA

ARTICLE INFO

Keywords: L-glutamate GABA Electrochemical sensor Platinum black Microelectrode array Dual sensing

ABSTRACT

Real-time tracking of neurotransmitter levels *in vivo* has been technically challenging due to the low spatio-temporal resolution of current methods. Since the imbalance of cortical excitation/inhibition (E:I) ratios are associated with a variety of neurological disorders, accurate monitoring of excitatory and inhibitory neuro-transmitter levels is crucial for investigating the underlying neural mechanisms of these conditions. Specifically, levels of the excitatory neurotransmitter L-glutamate, and the inhibitory neurotransmitter GABA, are assumed to play critical roles in the E:I balance. Therefore, in this work, a flexible electrochemical microsensor is developed for real-time simultaneous detection of L-glutamate and GABA. The flexible polyimide substrate was used for easier handling during implantation and measurement, along with less brain damage. Further, by electrochemically depositing Pt-black nanostructures on the sensor's surface, the active surface area was enhanced for higher sensitivity. This dual neurotransmitter sensor probe was validated under various settings for its performance, including *in vitro*, *ex vivo* tests with glutamatergic neuronal cells and *in vivo* test with anesthetized rats. Additionally, the sensor's performance has been further investigated in terms of longevity and biocompatibility. Overall, our dual L-glutamate:GABA sensor microprobe has its unique features to enable accurate, real-time, and long-term monitoring of the E:I balance *in vivo*. Thus, this new tool should aid investigations of neural mechanisms of normal brain function and various neurological disorders.

1. Introduction

L-glutamate (Glu) and gamma-aminobutyric acid (GABA) are the most abundant excitatory and inhibitory neurotransmitters in the central nervous system of mammals, respectively. They are assumed to be involved in various neurological disorders including seizures, trauma, and autism spectrum disorder (ASD) (Guerriero et al., 2015; Kurian et al., 2011; Robinson et al., 2008; Sandberg and Garris, 2010). These affect vast amount of people worldwide and specifically for ASD, while one in 44 children were diagnosed with ASD (Maenner et al., 2021), the

cause for the disorder remains unsolved. However, recent studies indicate that there are changes not only in neurotransmitter levels individually but also in excitatory: inhibitory (E:I) neurotransmitter balances. The E:I imbalance could lead to the development of neurological disorders (El-Ansary and Al-Ayadhi, 2014; Gao and Penzes, 2015). For ASD, recent findings discovered specific brain pathology associated with it, such as overgrowth of dendritic spines that can lead to increased glutamatergic excitation and reduced numbers of GABAergic interneurons (Jones et al. 2019, 2020, 2021). This indicates the possibility of E:I imbalance in ASD patients and therefore, an efficient and reliable

^{*} Corresponding author. Electrical Engineering, Biomedical Engineering and Computer Science, University of California Irvine, Irvine, CA, 92697, USA. *E-mail address:* hungcao@uci.edu (H. Cao).

way to measure the amount of Glu and GABA *in vivo* in real time is highly in demand. Microdialysis has been commonly used for measuring neurotransmitters *in vivo*, with which a small catheter is inserted into the measurement site and solutes of interest cross the semipermeable membrane due to the concentration difference (Defaix et al., 2018; Reinhoud et al., 2013). However, since the analyte must diffuse through the membrane before being collected for analysis, the temporal resolution for this technique is very low to be used for studying the mechanism of neurotransmitter release related to social behaviors (Denoroy and Parrot, 2018; Saylor et al., 2017). In addition, the spatial resolution is limited by the size of the catheter required. Alternatively, electrochemical sensors using microelectrode arrays (MEAs) have been gaining attention for its second-by-second detection with submillimeter spatial resolution within the brain (Hascup et al., 2007).

Till date, many groups have reported electrochemical neurotransmitter sensors for various molecules, including dopamine, acetylcholine, Glu, and GABA, just to name a few (Fenoy et al., 2020; Kiyatkin and Wakabayashi, 2015; Lin et al., 2014; Liu et al., 2020). Specifically, for Glu and GABA, enzyme-based sensors targeting each single neurotransmitter were developed in depth (Alamry et al., 2020; Ganesana et al., 2019; Wen et al., 2019). However, for dual sensing of Glu and GABA, there have been only a few (Burmeister et al., 2020; Hossain et al., 2018; Moldovan et al., 2021). The main reason is for GABase (the enzyme used for GABA sensors) to react with GABA, a precursor namely alpha-ketoglutarate (α-keto), is required. But since the discovery that the α -keto is actually one of the products from the Glu reaction, only few groups have reported a dual Glu:GABA sensor without the need for external α-keto (Burmeister et al., 2020; Hossain et al., 2018; Moldovan et al., 2021). As shown in Fig. 1, the α-keto required for the GABA reaction to occur is replenished by the Glu reaction and the final reporting molecule, H₂O₂, gets oxidized on the sensor's surface. Nevertheless, the dual Glu:GABA sensors recently reported still possess drawbacks to be significantly improved for reliable real-time in vivo measurements (Billa et al., 2022; Burmeister et al., 2020; Doughty et al., 2020; Hossain et al., 2018; Moldovan et al., 2021). All of those utilized rigid substrates such as ceramic or silicon. However, because of the sensor's small dimensions, it is prone to break during implantation and this brittleness makes the sensors challenging to handle throughout neurotransmitter monitoring process. Furthermore, detection in 2D platforms such as in cell cultures is unfeasible since these does not provide enough depth for the sensor to be inserted without breaking it. Another drawback of the

dual neurotransmitter sensors reported so far is that the sensing surface of the sensors are bare platinum (Pt). This bare surface holds a low active surface area, which is proportional with the sensory output (in ampere-A) in tens of pA. This calls for a strategy to achieve higher sensitivity to better distinguish the small amount of neurotransmitter level changes. To address these limitations, we propose to utilize flexible substrate for handling and to form nanostructures on the sensing surface to enhance the performance

In this paper, we introduce a flexible integrative dual Glu:GABA sensor with high sensitivity which can support a variety of neuroscience studies. To improve the performance, the biosensor was fabricated on a flexible polyimide substrate and Pt nanostructures were electrodeposited to increase the active surface area. By providing more space for the molecules to react on, the overall current increases allowing enhanced sensitivity. Additional unique features include longevity and biocompatibility enhancement. The sensor microprobe was validated *in vitro*, *ex vivo* and *in vivo* showing promising results to be further deployed for studies.

2. Materials and methods

2.1. Materials

Phosphate buffered saline (10X PBS), glutaraldehyde, and 30% hydrogen peroxide (H₂O₂) were purchased from Thermo Fisher Scientific (Waltham, MA). 97+% L-glutamic acid monopotassium salt monohydrate, 99.9% dihydrogen hexachloroplatinate(IV) hydrate hydrate, 99% dopamine hydrochloride (DA), and 97% bovine serum albumin (BSA) were purchased from Alfa Aesar (Haverhill, MA). L-ascorbic acid (AA), 99% m-phenylenediamine dihydrochloride (mPD), 98% potassium ferricyanide, and 99+% gamma-aminobutyric acid (GABA) was purchased from Acros Organics (Fair Lawn, NJ) and glutamate oxidase (GOx) from US Biological Life Science (Swampscott, MA). GABase and sodium pentobarbital were purchased from Sigma Aldrich (St. Louis, MO). Isoflurane was from Pivetal (Loveland, CO), and atropine sulfate was from Vedco (Saint Joseph, MO).

2.2. Microelectrode array design and fabrication

The samples were first fabricated at University of California Irvine's Integrated Nanosystems Research Facility (INRF). Flexible 125- μ m-thick

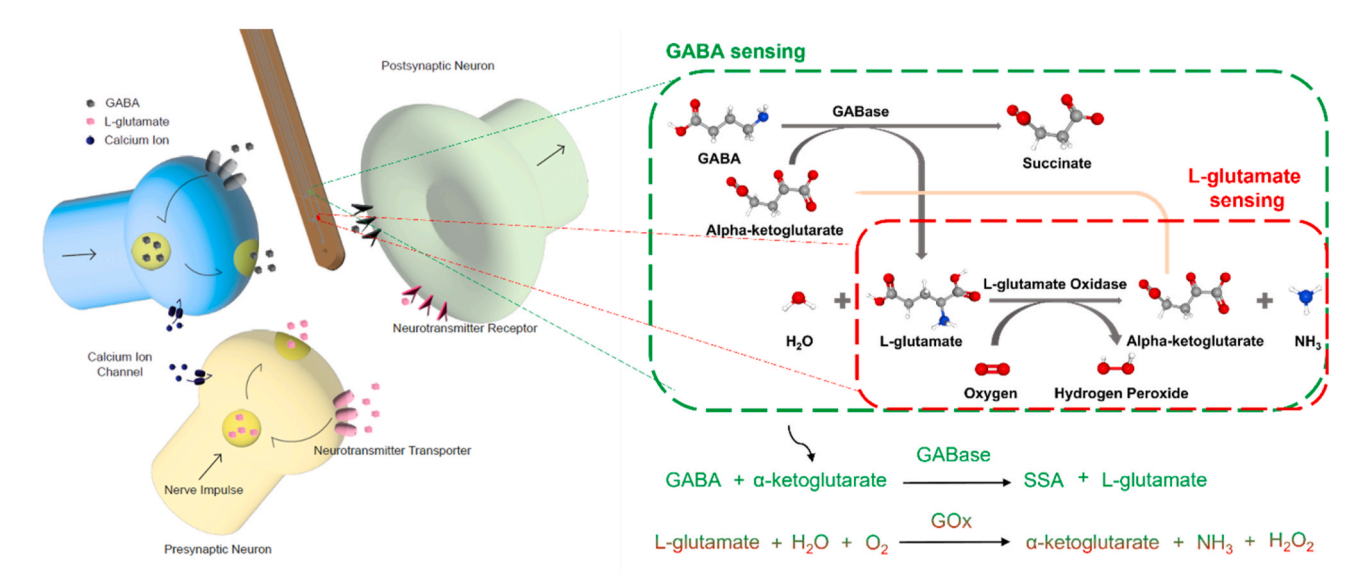


Fig. 1. Schematic diagram for L-glutamate and GABA sensing. The dual L-glutamate: GABA sensor detects the neurotransmitters released to the extracellular space through specific enzymatic reactions. The alpha-ketoglutarate required for GABase reaction is supplemented via the L-glutamate oxidase reaction, making dual sensing possible without the need for any external molecules.

polyimide films were cleaned with acetone, isopropyl alcohol (IPA) and deionized water (DI water) sequentially to remove any organic particles that might be present on its surface and dried with nitrogen gas. Then negative resist, NR9, was spin-coated on top of the polyimide followed by an ultraviolet (UV) light exposure to pattern the electrode layer. Onto the pattern, 20 nm of chromium (Cr) and 200 nm of either gold (Au) or platinum (Pt), were deposited with electron beam evaporator following the conditions listed in Supplementary Fig. S1. Cr serves as an adhesion layer for platinum to adhere to the polyimide substrate. Then the traces and the pads were defined using a lift-off process, where an inverse pattern of sacrificial layer (NR9) is patterned before the metal deposition and lifted-off after the e-beam, leaving the target material only in the regions with direct contact. Afterwards, a barrier layer was made with SU-8 2000 to separate the sensing pads from the connecting traces. With heating and developing, the initial form of the sensor was obtained in a batch within 4-inch circular polymer samples, where it was sent to LASEA Inc. (El Cajon, CA) for laser cutting. The final form of the sensor after laser-cutting has a width of 495 μm and consists of five 50 μm \times 100 µm electrodes (Supplementary Fig. S2), where the one in the middle is for pseudo-referencing, two on the right each refers to Glu and GABA sensing, and the two placed across from them are the self-referencing pads for the two neurotransmitters.

2.3. Surface modification for neurotransmitter detection

For the electrodeposition of Pt nanostructures (or Pt-black), first, 0.01-M chloroplatinic acid was made by dissolving chloroplatinic acid hydrate ($\rm H_2PtCl_6 \bullet H_2O$) in DI water. Then potential ranging from -0.4 to +0.8 V vs. a Ag/AgCl reference electrode was cycled with a scan rate of 50 mV/s for 10 cycles. A commercial potentiostat from CH Instruments was used (700 E, CH Instruments, Austin, TX) for the process and once the electrodeposition was accomplished, the sensors were rinsed with DI water and kept in air to dry before enzyme deposition.

Next, enzymes of interest were deposited on the sensing electrodes. First, 10 mg of BSA was dissolved in 985 µl of DI water followed by mixing 5 µl of glutaraldehyde into the BSA solution as a crosslinking agent. After inverting it manually 5 times, the solution was left at room temperature for 5 min for BSA to bind to one of the arms of glutaraldehyde. Meanwhile, the aliquoted enzymes stored in -80°C were brought out to room temperature for thawing. Depending on the target neurotransmitter, either 0.5 μl of GOx (1U/1 $\mu l)$ or 0.5 μl of the GOx and 0.5 ul of the GABase (1U/1 μ l) were mixed with the BSA solution to make a total volume of 5 μ l, where the amine groups of the enzymes bound to another arm of glutaraldehyde. As for the mixtures applied on the self-referencing pads, the composition of solutions was the same except for the lack of enzymes for the target neurotransmitter. In short, the self-referencing pad for Glu lacked GOx and for GABA lacked GABase. Once the solution is ready, the probes are placed under a stereotactic microscope for enzyme immobilization. Using 50 µl Hamilton's syringe, the enzymatic solution was drawn and manually deposited on the sensing pads of interest. For each pad, 3 applications in total were made by drop casting the solution (approximately 0.05 µl/drop). Between each application, 1 min interval was given for the solution to settle and once all the deposition has been completed, the probes were stored in the refrigerator at 4°C for at least 2 days for curing.

Lastly, an exclusion layer was formed on the surface for the sensor's selectivity. mPD, known to block the interferent molecules via size exclusion, was adapted to repel other electroactive molecules that are present in brain and cause interference, such as AA and DA (Wahono et al., 2012; Zhou et al., 2010). A solution of 0.05 M PBS was deoxygenated by purging with nitrogen gas for 20 min followed by dissolving mPD to make the final concentration of 5 mM. Inside a fume hood, the enzyme deposited probes were immersed in the mPD solution and a potential between +0.2 and +0.8 V vs a Ag/AgCl reference electrode was cycled for 15 min. Once the deposition was done, the probes were rinsed with DI water and kept at 4°C for at least 24 h before calibration.

The overall sensor fabrication process is shown in Supplementary Fig. S3.

2.4. Characterization and calibration

To quantify the increase in the sensor's active surface area through Pt-black deposition, the Randles-Sevcik equation was used. The equation is commonly used to describe the effect of scan rate on the peak current, but it also relates the peak current with the electrode surface area (Zaib and Athar, 2018), assuming a room temperature condition

$$i_p = (2.69 \times 10^5) n^{\frac{3}{2}} A D^{\frac{1}{2}} v^{\frac{1}{2}} C \tag{1}$$

where i_p is the peak current, n is the number of electrons transferred in the redox reaction (1 in this case), A is the electrode area in cm², D is the diffusion coefficient in cm²/s, C is the concentration in mol/cm³, and v is the scan rate in V/sec. The peaks of the waveform were calculated by using the $K_3Fe(CN)_6$ as the redox couple for cyclic voltammetry. 5 mM of $K_3Fe(CN)_6$ in 0.1 M KCl was prepared and the probes were immersed in the solution. With a scan rate of 50 mV/s, potential between -0.2 and +0.6 V vs. a Ag/AgCl reference electrode was cycled. From the resulting cyclic voltammogram, the peaks of the current were extracted and substituted into the equation to calculate the active surface area.

For the sensor's performance validation, a multichannel potentiostat from Pinnacle Technology Inc. (8102-N, Lawrence, KS) was used for measurement. A solution of either 1X PBS (for Glu) or 1 mM alphaketoglutarate (for GABA) was placed onto a hot plate to provide 37° C. Then the probes were immersed into the solution while applying +0.7 V against a glass Ag/AgCl reference electrode (RE) with constant magnetic stirring for uniform diffusion. Various concentrations of Glu and GABA were dropped into the solution to achieve the sensitivity plot and additional molecules such as AA, DA, and H_2O_2 were introduced to test for selectivity. For deriving the limit of detection (LOD), 3 times the standard deviation of the baseline was divided by the least squares slope.

2.5. Ex vivo experiments

For sensor validation with glutamatergic neuronal cells, the cells were prepared by derivation from human induced pluripotent stem cells (iPSCs). iPSCs were first cultured on Matrigel coated microplates and differentiated to neural progenitor cells (NPCs) for three weeks, using a commercial differentiation medium based on dual-SMAD inhibition (Neural Induction Medium, StemCell Technologies). Afterwards, NPCs were differentiated into glutamatergic neurons using neural differentiation medium (NDM; composed of neurobasal medium, 2% B-27, 200 μM ascorbic acid, and 1% Glutamax, Gibco) for 10 days at a 70% confluency. Finally, human iPSC derived astrocytes were mixed with the NPCs to establish a stable long term monolayer co-culture. Note that differentiation of human iPSCs to astrocytes was undertaken following the method from Serio et al., (2013), including exposure of NPCs to leukemia inhibitory factor (LIF), followed by fibroblast growth factor (FGF2), and ciliary neurotrophic factor (CNTF) over a 3-month period. After mixing astrocytes and the partially differentiated NPCs, differentiation of the NPCs into glutamatergic neurons continued for an additional 20 days using NDM supplemented with 1% N2 (Gibco). Subsequently, the neuron-astrocyte co-culture was maintained in NDM with 1% N2 for at least a month before they were used for glutamate activity measurements.

To maintain the neuronal cell's activity during the measurement, artificial cerebrospinal fluid (aCSF) was prepared before the experiment for the glutamatergic neurons. Chemicals were mixed to obtain the final composition of 125 mM NaCl, 26 mM NaHCO $_3$, 1.25 mM NaH $_2$ PO $_4$, 4 mM glucose, 3 mM KCl, 1 mM MgCl $_2$, and 2 mM CaCl $_2$ in DI water. Once evenly mixed, the solution was filtered with 0.22 μm filter apparatus to filter out any biological debris and stored in 4°C until further use.

At the day of the experiment, neurotransmitter sensors were

validated *in vitro* prior to *ex vivo* testing and all the solutions required for the experiment was put into a water bath to match 37°C before use. Cells were placed on a hot plate to maintain a constant temperature of 37°C and the cells were washed twice with aCSF after removing the culture medium. With the cells in aCSF, the neurotransmitter sensor and a AgCl/Ag wire pseudo-RE was placed in proximity using stereotaxic holders. Constant potential of +0.7 V was applied with the 8102-N multichannel potentiostat from Pinnacle Inc., and 15 to 20 min of stabilization period was given. Once ready for recording, filtered 70 mM KCl with a composition of 70 mM KCl, 79 mM NaCl and 2.5 mM CaCl $_2$ in DI water (pH 7.4) was locally applied to stimulate the glutamatergic neurons (Burmeister et al., 2020; Hascup et al., 2007).

2.6. In vivo experiments

All animal protocols were reviewed and approved by Institutional Animal Care and Use Committee (IACUC) protocol (# AUP-21-079, University of California, Irvine). Male Sprague-Dawley rats were used for this study. Rats were anesthetized with 4% isoflurane until a toepinch reflex is no longer present. A bolus of sodium pentobarbital (55 mg/kg, b.w.) was then injected interperitoneally. Atropine sulfate (0.05 mg/kg, b.w.) injection was followed to help reduce the secretions to facilitate breathing. Then, a rectal probe was inserted to monitor and maintain the rat's body temperature using heating blanket's feedback system. To expose the recording site, a midline incision was made and after resection of the underneath tissue craniotomy and durotomy of 2 mm × 2 mm were made over the rat's primary somatosensory cortex. The dual Glu:GABA sensor was lowered in the cortical layer 4 of the rat's primary barrel cortex and a constant potential of +0.7 V was applied against a AgCl/Ag wire pseudo-RE. During the recording, the rats were supplemented with sodium pentobarbital (14 mg/kg, b.w.) every 45 min or as required to maintain steady anesthesia. After a stabilization period of 30 to 40 min for baseline establishment, through glass micropipettes that were attached to the sensor platform (Supplementary Fig. S4), local injection of 70 mM KCl was given to stimulate brain extracellular space using Microinjection Syringe Pump (World Precision Instruments, Sarasota, FL). For the recordings, the Tethered Mouse System from Pinnacle Technology Inc. (8400-K1, Lawrence, KS) was used. A simplified schematic of the setup is shown in Supplementary Fig. S5.

2.7. Surface modification for biocompatibility comparison

To test for the biocompatibility among different RE materials, IrOx and AgCl were coated onto the Pt probes. For IrOx coating, oxalate-IrCl₄ plating solution (Yamanaka solution) was prepared with a composition of 0.14% IrCl₄, 99.36% water, and 0.50% $C_2H_6O_2$. Then using potassium carbonate (K₂CO₃), the pH of the solution was adjusted to 10.5 and kept at room temperature for 3 days before use. For coating, the probes were immersed in the plating solution and a potential was cycled ranging from -0.8 V to +0.7 V against a glass Ag/AgCl RE for 50 times with a scan rate of 50 mV/s. For AgCl, Ag was first coated on the probe using Transene Ag plating solution. With the Pt probe immersed in the solution, constant cathodic current of 0.02 mA was applied against a Pt counter electrode (CE) for 60 s and rinsed with water. Then the Ag coated probes were put in a 1 M KCl solution, and an anodic current of 0.05 mA was applied against a Pt CE for 5 min to coat AgCl. After the deposition, the probes were rinsed with DI water and set aside for further enzyme deposition following in vitro testing.

3. Results and discussion

3.1. Material optimization for its oxidative properties

To enhance the sensitivity our dual Glu:GABA amperometric sensors, one of the approaches is to increase the active surface area and this can be explained by the Cottrell equation (Rezaei and Irannejad, 2019):

$$i = \frac{nFAc_0\sqrt{D}}{\sqrt{\pi t}} \tag{2}$$

where i is the current (A); n is the number of electrons transferred; F is the Faraday constant (F = 96,487 C mol⁻¹); A is the surface area of planar electrode (cm²); c_0 is the initial concentration of the analyte (mol•mL⁻¹); D is the diffusion coefficient (cm²•s⁻¹); t is the time elapsed since the potential was applied (s). Since the current is proportional to the surface area of the planar electrode, to increase the active surface area for higher current response, electrodeposition of nanostructures, specifically Pt, was chosen. Because Pt is a very costly noble metal, electrodeposition of the material provides a facile and cost-effective way to form nanostructures on the sensor surface (Chu et al. 2021a, 2021b). This method specifically lets Pt to be adhered to the electrode surface with no spare Pt being wasted, yielding the optimal output in a cost-effective manner. Also, surface modification via electrochemical deposition can be monitored during the process and the consistency throughout multiple probes can be validated by looking at the resulting cyclic voltammogram.

To validate the increase of surface area through electrodeposited Ptblack nanoparticles, scanning electron microscopy (SEM) and quantification of the surface area through electrochemical measurements were performed. As shown in Fig. 2A, Pt-black nanostructures were observed for the samples after deposition, but for bare Pt, just a plain metal surface was observed. Thus, nanostructure formation was confirmed through optical validation via SEM (Tescan GAIA3, Brno-Kohoutovice, Czech Republic). Then, to further validate the surface area enhancement, the active surface area of the samples was quantified using Randles-Sevcik equation. Potassium ferricyanide (K₃Fe(CN)₆) was used for the redox couple and cyclic voltammetry was performed to retrieve the peak currents to derive the surface area. When substituting the peak current from the cyclic voltammogram shown in Fig. 2B to the Randles-Sevcik equation, the calculated active surface area of Pt-black coated Pt was about 1.8 times higher than that of the bare Pt probe (from 4207.07 μm^2 to 7567.33 μm^2). Thus, using both optical and electrochemical validation through SEM and cyclic voltammetry, it was shown that the electrodeposition of Pt-black nanostructures efficiently enhances the surface area of the electrodes

Then, the sensors' performance towards H₂O₂ oxidation was tested. H₂O₂ is the reporter molecule for the enzymatic reaction used for Glu and GABA and this gets oxidized by the polarized sensor surface, generating current (Fig. 1). Thus, various combinations of materials (bare Au, bare Pt, Pt-black deposited Au, and Pt-black deposited Pt) were compared and tested to find the best metal layer to be used for the dual Glu:GABA sensor (Fig. 2C). Au is a widely used metal for electrophysiological studies, such as electrocardiogram (ECG) and electroencephalogram (EEG) measurement, and Pt is known for its superior electrochemical activity during redox reactions compared to other noble metals (Hamdan and Zain, 2014). Thus, these two metals with and without Pt-black surface modification were chosen to be compared for their oxidative properties towards H₂O₂. As expected, for both Au and Pt, Pt-black deposited surfaces showed higher sensitivity towards H₂O₂ when compared to the bare ones, showing the effect of increase in surface area through Pt-black nanostructures contributing to sensitivity enhancement. Further, even bare Pt showed higher responses than Pt-black deposited on Au confirming Pt's superior oxidation capabilities towards H2O2. Overall, Pt-black deposited on Pt showed the highest sensitivity, and so, this composition was selected as our sensing material for the experiments that follows.

3.2. In vitro validation for sensitivity and selectivity

To validate the fabricated sensor for Glu and GABA detection, it was first calibrated (*in vitro* testing). Self-referencing strategy was used on the microelectrode array probe, where there is another recording site close to the actual recording site that monitors any other signal except

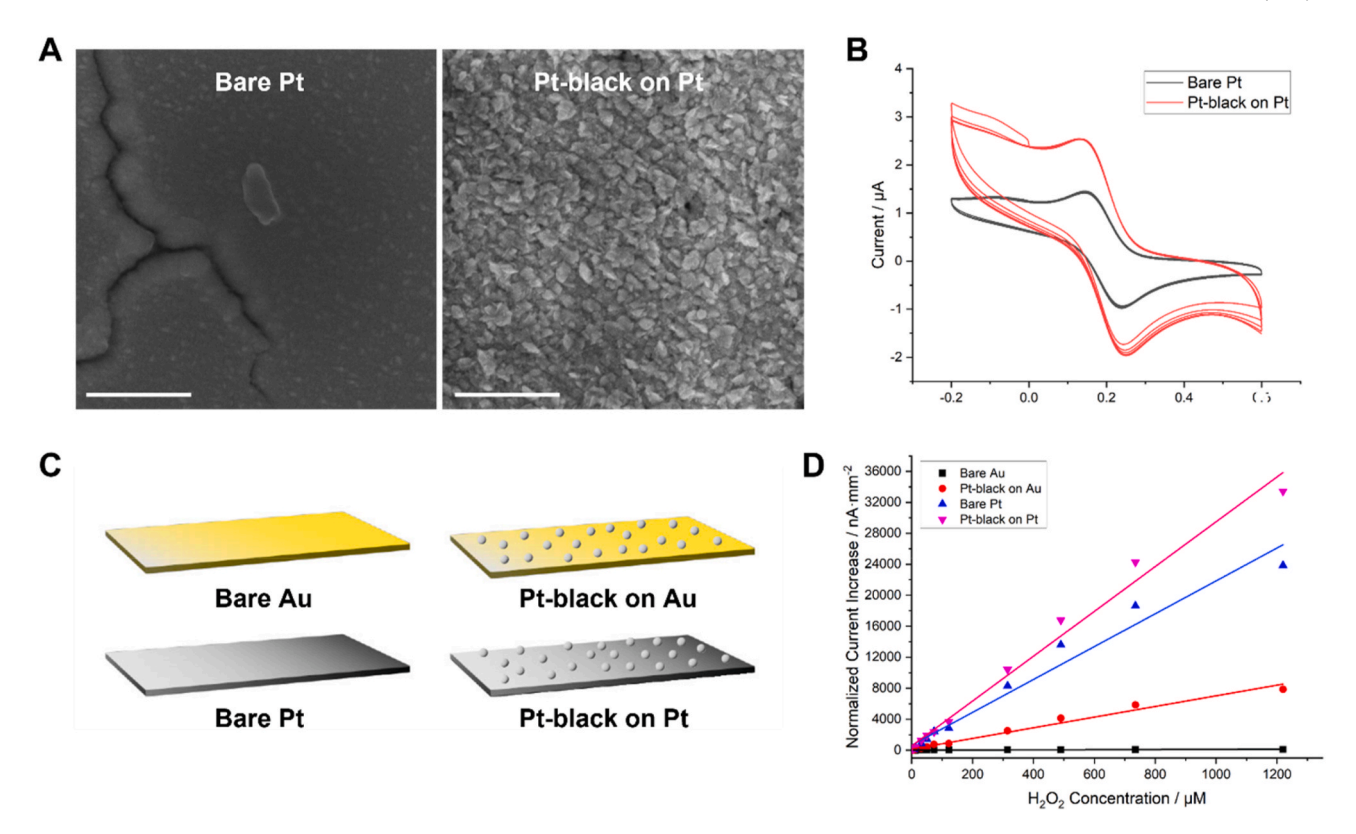


Fig. 2. Material optimization. A. Scanning Electron Microscopy (SEM) images for bare Pt and Pt-black electrodeposited on Pt, showing the nanostructures deposited through the Pt-black deposition (Scale bar = 1 μ m). B. Cyclic voltammograms for the two probes using $K_3Fe(CN)_6$ as the redox couple. C. Four different compositions of metals tested for oxidative properties towards H_2O_2 . D. H_2O_2 sensitivity calibration curve for the four compositions (sensitivity: Pt-black on Pt > Bare Pt > Pt-black on Au > Bare Au).

for the target molecule (Cao et al., 2012). Briefly, the self-referencing site has the identical dimensions and composition as the sensing site but excluding the enzyme that reacts with the target neurotransmitter. By having a site with a blank enzymatic layer with similar thickness next to the sensing site, the self-referencing site receives the same ambient noise as the sensing site. Thus, for example, as shown in equation (3), while the L-glutamate sensing (working) electrode detects the current generated from Glu along with the Faradaic and non-Faradaic currents that are caused by other electroactive molecules that reaches the sensing surface, the self-referencing site detects all the noises excluding the current from Glu. These two signals can later be subtracted to enhance the signal-to-noise ratio (SNR), eliminating any signals that are generated from other molecules and interferences aside from the target.

$$\begin{split} i_{working} &= i_{Glu} + (i_{F1} + i_{F2} + \dots + i_{Fn}) + (i_{nonF1} + i_{nonF2} + \dots + i_{nonFn})i_{self-ref} \\ &= (i_{F1} + i_{F2} + \dots + i_{Fn}) + (i_{nonF1} + i_{nonF2} + \dots + i_{nonFn})i_{Glu} \\ &= i_{working} - i_{self-ref} \end{split}$$

To find out our sensor's Glu sensitivity, the probes were immersed in $37^{\circ}C$ 1X PBS with magnetic stirring while known concentrations of Glu ranging from 5 to $100~\mu\text{M}$ were dropped in the beaker sequentially. From the resulting current increase (Supplementary Fig. S6A), the sensitivity for Glu was analyzed and the limit of detection was calculated by dividing the 3 times the standard deviation of the baseline by the least squares slope. As in Fig. 3A, Glu sensor with surface area enhancement through Pt-black deposition showed a good linearity towards Glu with a sensitivity of 1.74 nA mm $^{-2}\mu\text{M}^{-1}$ (R $^2=0.991$) and a limit of detection (LOD) of 0.12 μM . GABA sensitivity was validated similarly, where in this case, 1 mM α -ketoglutarate solution was used instead of 1X PBS due to the need of a precursor for the GABase reaction to occur. Known concentrations of GABA was added ranging from 10 to 100 μM

(Supplementary Fig. S6B) and as in Fig. 3B, GABA sensor with surface area enhancement through Pt-black deposition showed a good linearity with a sensitivity of 1.34 nA mm $^{-2}\mu M^{-1}$ (R $^2=0.968$) and a LOD of 0.04 μM , which is more sensitive than the previously reported sensors with bare Pt working electrode

After validating its sensitivity, the sensors were subjected to a selectivity test for its specificity towards GABA. The experimental setup was similar to the sensitivity tests but interference molecules such as 250 μM AA and 2 μM AA were added along with Glu and GABA. As shown in Figs. 3C and D, addition of the target neurotransmitters (20 μM Glu and GABA) generated current only at the sensing and not at the self-referencing site, showing the sensor's specificity. For the interferents, there was no increase in current for both sites showing the effective repelling of molecules by the mPD layer. Finally, when the products of the enzymatic reaction were introduced (9 μM H₂O₂ for Glu and Glu for GABA), signals were observed at both sites, which the signal from self-referencing can later be subtracted from the sensing to increase the signal-to-noise ratio (SNR).

3.3. Ex vivo validation

Further validation *ex vivo* with neuronal cell culture was performed before implanting the probes *in vivo*. As shown in the diagram (Fig. 4A), the iPSCs were differentiated for 3 weeks into NPCs, where the NPCs were further cultured for 2 weeks to reach a stable status. Lastly, astrocytes were mixed with the NPCs and grown for 10 days to provide the stimulation that they need to achieve the excitatory glutamatergic neurons. To confirm that the cells successfully differentiated into glutamatergic neurons, the cells were stained with DAPI, glial fibrillary acidic protein (GFAP), and β 3T. As shown in Fig. 4B, DAPI staining showed the survival of the cells, GFAP showed reactive astrocytes in the culture, and β 3T indicated that the differentiated cells are neurons.

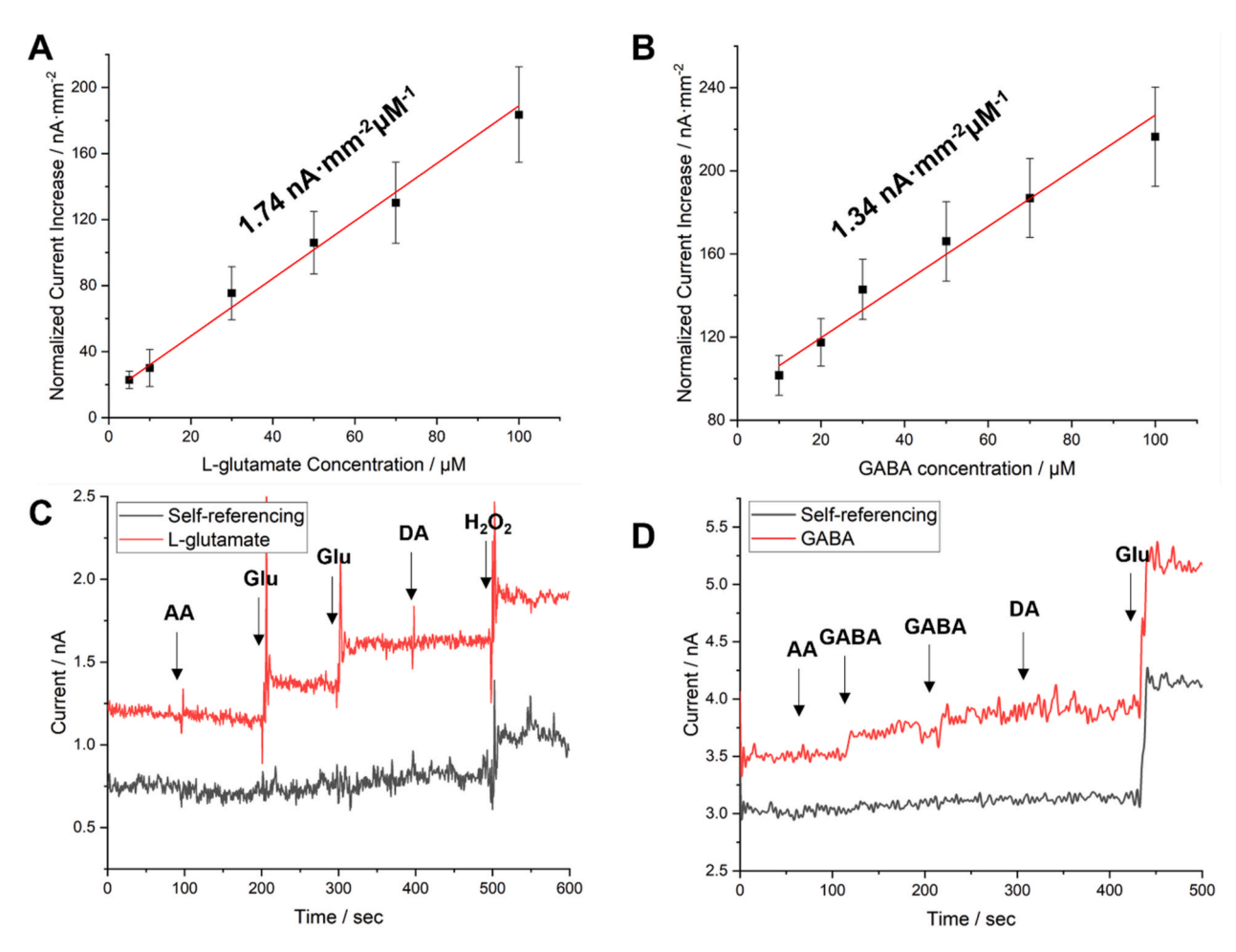


Fig. 3. In vitro validation of dual L-glutamate: GABA sensor. Calibration curve with sensitivity for A. L-glutamate ranging from 5 to 100 μ M and B. GABA ranging from 10 to 100 μ M (n = 4). Selectivity test for C. L-glutamate and D. GABA with addition of interferent molecules (ascorbic acid and dopamine). The sensing sites for L-glutamate and GABA only react to the target neurotransmitters while the self-referencing sites do not show any increase, showing the sensor's specificity. No significant current increase was observed for the interferent molecules (AA and DA), indicating the sensor's selectivity.

Once the cell culture platform of glutamatergic neurons was ready for measurement, the neurotransmitter sensors were tested for Glu detection. The cells were kept at 37°C and aCSF to maintain its activity during measurement and 70 mM of KCl was added locally to the cells for stimulation after establishing a stable baseline. As in Fig. 4C, following KCl stimulation, there was a sharp increase in Glu signal within 10 s while no observable current change occurred at the self-referencing site, indicating that the sensor successfully detected Glu signal from the glutamatergic neurons. Also, based on sensor calibration, it was found that 70 μM of Glu was released from the glutamatergic cells from the stimulation

3.4. In vivo validation

After the sensors were validated *in vitro* and *ex vivo*, the sensors were finally tested *in vivo* to investigate its performance for dual Glu:GABA sensing. Using a stereotaxic holder, the dual Glu:GABA sensor was inserted into cortical layer 4 of the rat's primary barrel cortex. The recording started after giving it around 30 min of stabilization time and with 70 mM KCl stimulation, current changes in both GABA and Glu were observed. As shown in Fig. 5, sharp increases in current were noticed for both GABA and Glu, with the GABA signal being higher than that of Glu. Based on the design of the sensor, GABA sensing pad reacts to both GABA and Glu, while the Glu sensing only monitors the Glu level in the extracellular space. Thus, when the signal from Glu sensing pad is subtracted from that of GABA sensing, it would indicate the amount of

current change generated from GABA release. Overall, from the two chemical stimulation sessions, a consistent increase in currents was observed for both Glu and GABA, where these correlate to 11.98 μM of Glu and 29.63 μM of GABA in the area of interest

3.5. Additional features for the sensor performance

Sensitivity and selectivity are among the most important features when developing a sensor platform but considering the fabrication process and the specific purpose for detecting neurotransmitters in vivo for a long period of time, there were other aspects that needed to be thought out regarding the dual Glu:GABA sensor. First, the longevity of the sensor was investigated to better understand the sensor's lifetime with the optimal period that the sensor can be used for. Since the dual Glu:GABA sensor utilizes enzymes (Gox and GABase), the sensor's lifetime is highly dependent on the lifetime of the enzymes applied on the sensor which is relatively short (Moreira et al., 2017; Ou et al., 2019; Weltin et al., 2016). Thus, the longevity of the sensors was evaluated, where two storage conditions were compared to find the optimal method to keep the neurotransmitter sensors. The sensors were divided into two groups, where one was stored in ambient air and the other in 1X PBS. They were tested every two days for its response to 20 μM Glu and the results are shown in Figs. 6A and B. For both conditions, the sensors were able to detect Glu for more than 3 weeks. However, the sensitivity of the sensors kept in ambient air decreased faster than that of PBS, indicating that the sensors kept in PBS maintained its activity better.

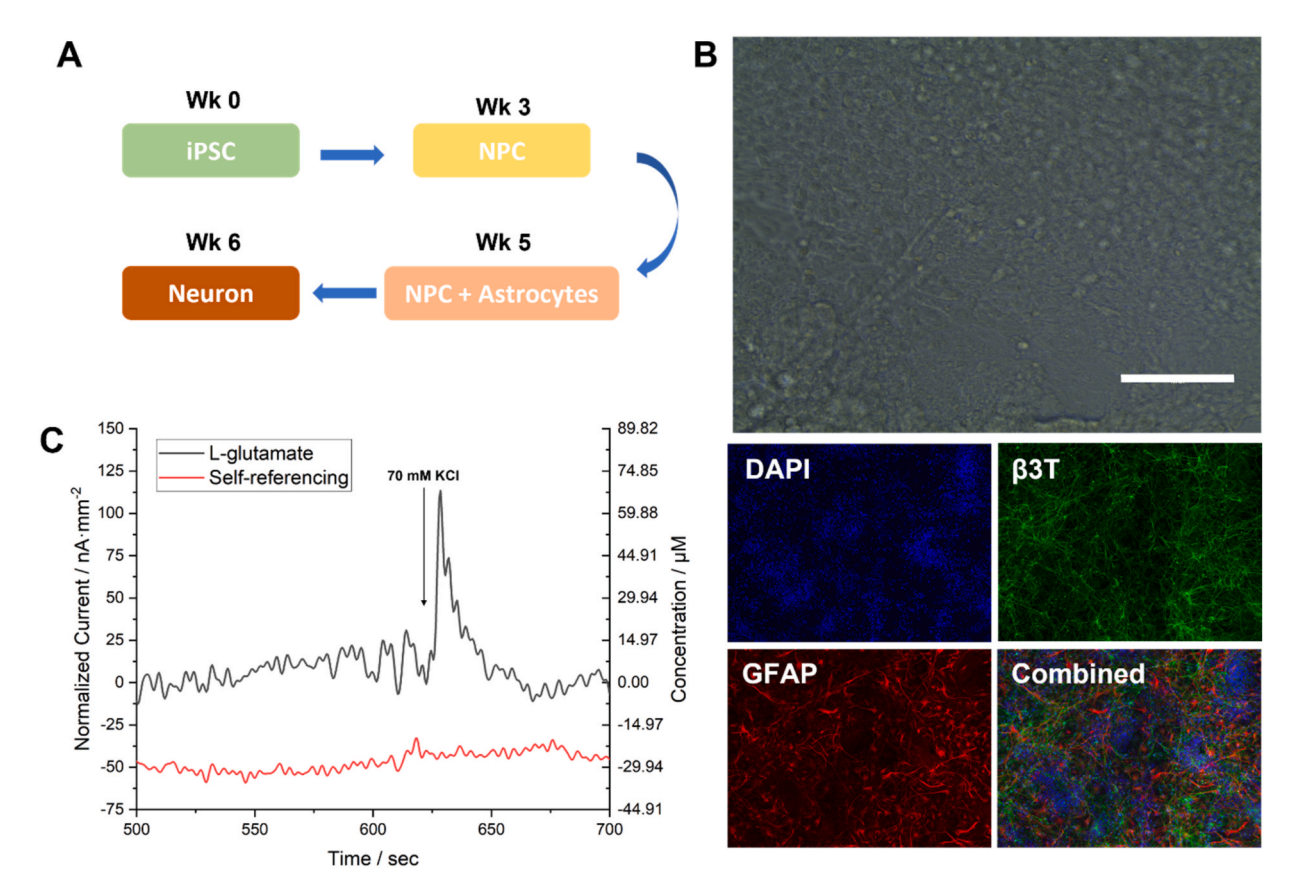


Fig. 4. Ex vivo recording. A. Glutamatergic neuron culture process. B. Optical images of the differentiated glutamatergic neuron and cell staining (Scale bar = $100 \mu m$). C. L-glutamate detection using the fabricated sensor showing the signals at L-glutamate sensing site and self-referencing site. The y axis on the right shows the L-glutamate concentration correlating to the current based on the calibration curve.

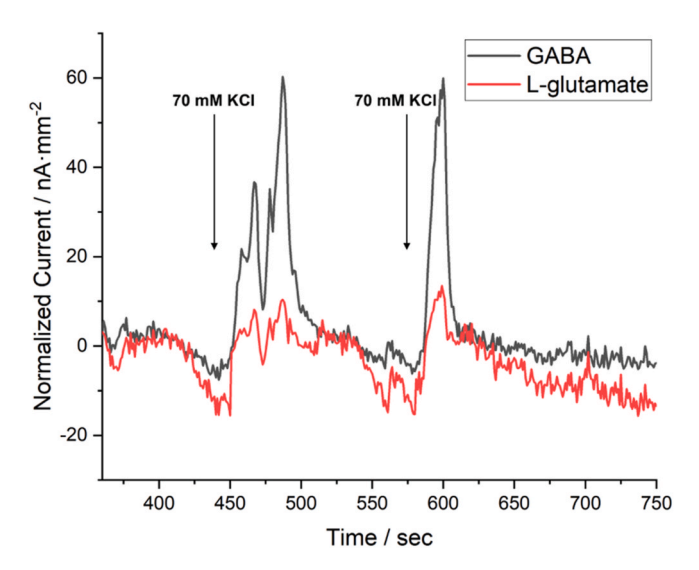


Fig. 5. In vivo recording. L-glutamate and GABA signals from 70 mM KCl stimulation in an esthetized rat's brain. While the L-glutamate sensing pad records the L-glutamate signal, since GABA sensing pad has both L-glutamate oxidase and GABase on the surface, it records signals from both L-glutamate and GABA. Thus, the signal from L-glutamate sensing pad needs to be subtracted from GABA sensing pad to retrieve the signal from GABA. The sensor showed a similar level of current increase for both GABA and L-glutamate to the consecutive stimulation, which corresponds to 11.98 μM of L-glutamate and 29.63 μM of GABA.

This can be from the fact that keeping the sensor in 1X PBS helps the enzymes maintain their physiological properties, while keeping them in ambient air with room temperature can dehydrate the enzymes. Also, the sensors in PBS showed longer longevity for about a month when the ones in ambient air lost their activity after 20 days. This result shows that keeping the sensors in PBS is a more effective method. This also helps speculate that once implanted *in vivo*, the sensors would be good for about a month

Another aspect being investigated was the flexibility of the sensor. While there are other dual Glu:GABA sensors the have been reported, they were all based on the ceramic substrate. While ceramic can provide rigidity and easy handling during the fabrication process, it is also fragile during implantation. Our experiences showed that it is very easy to break silicon and ceramic probes accidently. This is not only very costly but also extremely inconvenient as the entire experiment will be ruined by such incident. Thus, we chose flexible polyimide with an appropriate thickness (125 µm) as our substrate, where it does not break but can still penetrate the brain. The inset of Supplementary Fig. S7 shows how flexible the developed sensor is. To check if the sensor still maintains its sensitivity after being bent continuously, the neurotransmitter sensor has been subjected to a sensitivity test before and after bending at 70° for 100 times. As seen in Supplementary Fig. S7, the sensor maintained 93% of its sensitivity after bending, indicating that the sensor can withhold the distortion during implantation and animal movements during the measurements.

Lastly, the biocompatibility of the sensor was tested for *in vivo* applications. The REs commonly used for neurotransmitter detection *in vivo* are AgCl/Ag wire pseudo-REs. However, there has been some concerns on the biocompatibility of AgCl, stating that it can cause inflammatory response *in vivo* (Franklin et al., 2005). Also, implanting a whole another RE aside from the biosensor itself can cause more damage

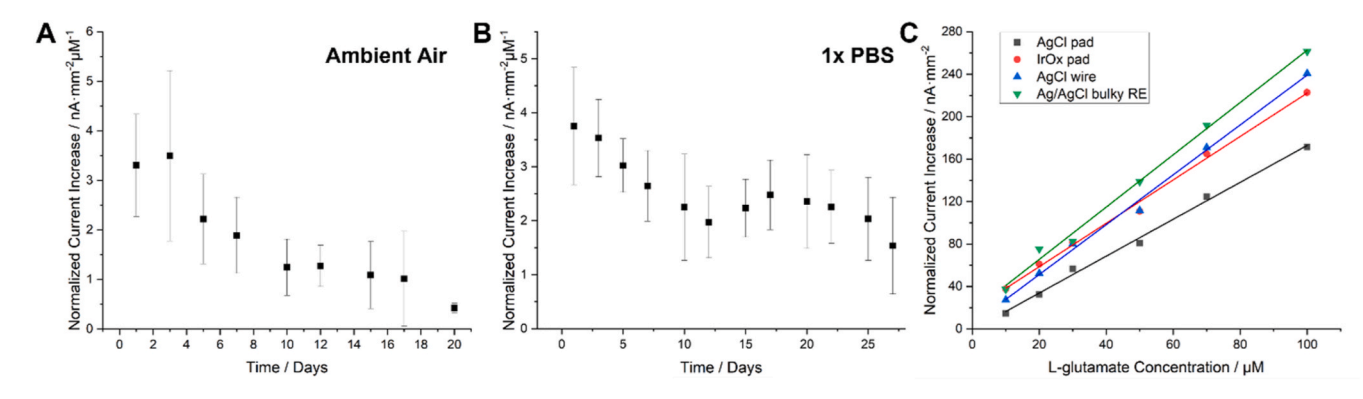


Fig. 6. Results for longevity and biocompatibility. The longevity of the enzymatic neurotransmitter sensor when kept at (A) ambient air, and in (B) 1X PBS, showing sensors in PBS shows higher longevity along with slower decrease in enzyme activity. C. The sensitivity plot for L-glutamate against 4 different reference electrode materials (Ag/AgCl bulky RE > AgCl wire > IrOx pad, AgCl pad).

to the brain. Therefore, a single probe that has both the working electrodes and the RE with higher biocompatibility would be better for the long-term measurements in vivo. Iridium oxide (IrOx) is one of the promising materials to be used as a RE material since the pH in the extracellular environment does not change much. In this regard, the performance of iridium oxide (IrOx) as a pseudo-RE material has been tested by checking its stability and comparing it with other REs that are available. First, to check the IrOx's stability as a pseudo-reference electrode material, it was subjected to an open circuit potential (OCP) test against a glass Ag/AgCl reference electrode for 24 h. As shown in Supplementary Fig. S8A, IrOx pseudo-RE (black) showed relatively stable potential in respect to commercial Ag/AgCl reference electrode (red) for the time tested. This result indicates the IrOx's capability of being used as a pseudo-RE for the dual Glu:GABA sensor. Then the actual performance of IrOx as a pseudo-RE for neurotransmitter detection was tested by comparing it with other RE materials. A total of 4 REs was compared: glass Ag/AgCl reference electrode, AgCl/Ag wire, AgCl coated Pt probe, and IrOx coated Pt probe. As shown in Supplementary Fig. S8B, Pt probes were specifically coated with IrOx and AgCl to have it integrated as the pseudo-RE. Then, the Glu sensitivity test was done and compared with 4 different RE materials and the result is shown in Fig. 6C. As expected, the bulky glass Ag/AgCl RE showed the highest sensitivity due to its high stability from the necessary chemicals supplied within the electrode, while AgCl coated pad showed the lowest. As for the others, IrOx pad and AgCl/Ag wire showed similar performance towards neurotransmitter sensing. Furthermore, cells were seeded on the AgCl and IrOx coated probes to compare the biocompatibility and as shown in Supplementary Fig. S8C, PNT1-A cells, an available line in the lab, on IrOx showed higher viability compared to the ones on AgCl probes. These results show that IrOx pseudo-RE can fully substitute for other pseudo-RE materials such as AgCl/Ag wire for in vivo studies with higher biocompatibility.

4. Conclusion and future works

In this study, a flexible dual Glu:GABA sensor with high sensitivity has been demonstrated for detecting neurotransmitters in the central nervous system for neurological studies. Using flexible polyimide as a substrate, the biosensor is easy to handle during implantation and measurements while maintaining its sensitivity. Further, Pt-black nanostructures were electrodeposited onto the sensing surface to increase the active surface area that leads to higher sensitivity towards Glu and GABA. The mPD coating along with self-referencing technique allowed target specific sensing. These advancements of the sensor were validated thoroughly in various settings, such as *in vitro* lab environments, *ex vivo* in glutamatergic neuronal cell cultures, and *in vivo* in the anesthetized rat. Additionally, we have provided novel strategies to enhance longevity and biocompatibility.

Overall, real-time monitoring of neurotransmitter level changes is highly in demand for studying the mechanisms behind neurological disorders. Not only does our dual Glu:GABA sensor can easily be used for monitoring the neuronal differentiation or any cell culture platform for neuroscience due to its flexibility, we specifically plan to apply our sensor to look at the mechanism of Glu:GABA imbalance related to early life sleep disruption (ELSD) models with relevance to E:I imbalance reported in autism spectrum disorder. Based on the recent findings regarding specific brain pathology associated with ASD, such as overgrowth of dendritic spines that can lead to increased glutamatergic excitation and reduced numbers of GABAergic interneurons (He et al., 2021; Jones et al. 2019, 2020, 2021; Manyukhina et al., 2022; Zhao et al., 2022), there is a possibility of E:I imbalance for ASD patients where further investigation is needed. The dual Glu:GABA sensor presented in this study can provide a tool for this purpose of detecting neurotransmitters in vivo with minimum brain damage with high sensitivity and this will bring the field a step closer to investigating the cause for neurological disorders.

Credit authorship contribution statement

Sung Sik Chu: Conceptualization, Data curation, Formal analysis, Investigation, Methodology, Writing – original draft, Writing – review & editing. Anh H. Nguyen – Conceptualization, Methodology. Derrick Lin: Cell culture. Mehwish Bhatti: Animal preparation. An Hong Do: Writing – review & editing. Ron D. Frostig: Writing – review & editing. Carolyn E. Jones-Tinsley: Conceptualization, Writing – review & editing. Zoran Nenadic: Writing – review & editing. Xiangmin Xu: Writing – review & editing. Miranda M. Lim: Conceptualization, Obtaining funding, Writing – review & editing. Hung Cao – Conceptualization, Methodology, Obtaining funding, Writing – review & editing. Writing – review & editing.

Declaration of competing interest

The authors declare that they have no known competing financial interests or personal relationships that could have appeared to influence the work reported in this paper.

Data availability

No data was used for the research described in the article.

Acknowledgement

The authors would like to acknowledge the financial support from the NSF CAREER Award #1917105 to H.C. and the NSF NCS Award #1926818 to H.C. and M.M.L.

Appendix A. Supplementary data

Supplementary data to this article can be found online at https://doi.org/10.1016/j.bios.2022.114941.

References

- Alamry, K.A., Hussein, M.A., Choi, J.W., El-Said, W.A., 2020. J. Electroanal. Chem. 879. Billa, S., Yanamadala, Y., Hossain, I., Siddiqui, S., Moldovan, N., Murray, T.A., Arumugam, P.U., 2022. Micromachines-Basel 13 (7).
- Burmeister, J.J., Price, D.A., Pomerleau, F., Huettl, P., Quintero, J.E., Gerhardt, G.A., 2020. J. Neurosci. Methods 329, 108435.
- Cao, H., Li, A.L., Nguyen, C.M., Peng, Y.B., Chiao, J.C., 2012. Ieee Sens J 12 (5), 1618–1624.
- Chu, S.S., Marsh, P., Nguyen, H.A., Jones, C.E., Lim, M.M., Cao, H., 2021a. Ieee Eng Med Bio 7148–7151.
- Chu, S.S., Marsh, P., Nguyen, H.A., Olson, R., Jones, C.E., Lim, M.M., Cao, H., 2021b. Proc Ieee Micr Elect 551–554.
- Defaix, C., Solgadi, A., Pham, T.H., Gardier, A.M., Chaminade, P., Tritschler, L., 2018.

 J Pharmaceut Biomed 152, 31–38.
- Denoroy, L., Parrot, S., 2018. Neuromethods 130, Vii-Viii.
- Doughty, P.T., Hossain, I., Gong, C.G., Ponder, K.A., Pati, S., Arumugam, P.U., Murray, T. A., 2020. Sci Rep-Uk 10 (1).
- El-Ansary, A., Al-Ayadhi, L., 2014. J. Neuroinflammation 11.
- Fenoy, G.E., Marmisolle, W.A., Azzaroni, O., Knoll, W., 2020. Biosens. Bioelectron. 148. Franklin, R.K., Johnson, M.D., Scott, K.A., Shim, J.H., Nam, H., Kipke, D.R., Brown, R.B., 2005. Ieee Sensor, pp. 1400–1403.
- Ganesana, M., Trikantzopoulos, E., Maniar, Y., Lee, S.T., Venton, B.J., 2019. Biosens. Bioelectron. 130, 103–109.
- Gao, R., Penzes, P., 2015. Curr. Mol. Med. 15 (2), 146-167.
- Guerriero, R.M., Giza, C.C., Rotenberg, A., 2015. Curr Neurol Neurosci 15 (5).
- Hamdan, S.K., Zain, Z.M., 2014. Malays. J. Med. Sci. 21, 12–26.
- Hascup, K.N., Rutherford, E.C., Quintero, J.E., Day, B.K., Nickell, J.R., Pomerleau, F., Huettl, P., Burmeister, J.J., Gerhardt, G.A., 2007. Electrochemical Methods for Neuroscience.
- He, J.L., Oeltzschner, G., Mikkelsen, M., Deronda, A., Harris, A.D., Crocetti, D., Wodka, E.L., Mostofsky, S.H., Edden, R.A.E., Puts, N.A.J., 2021. Transl. Psychiatry 11 (1).
- Hossain, I., Tan, C., Doughty, P.T., Dutta, G., Murray, T.A., Siddiqui, S., Iasemidis, L., Arumugam, P.U., 2018. Front. Neurosci. 12, 500.
- Jones, C.E., Chau, A.Q., Olson, R.J., Moore, C., Wickham, P.T., Puranik, N., Guizzetti, M., Cao, H., Meshul, C.K., Lim, M.M., 2021. Curr Res Neurobiol 2.
- Jones, C.E., Opel, R.A., Kaiser, M.E., Chau, A.Q., Quintana, J.R., Nipper, M.A., Finn, D.A., Hammock, E.A.D., Lim, M.M., 2019. Sci. Adv. 5 (1), eaav5188.
- Jones, C.E., Wickham, P.T., Lim, M.M., 2020. Behav. Neurosci. 134 (5), 424-434.

- Kiyatkin, E.A., Wakabayashi, K.T., 2015. ACS Chem. Neurosci. 6 (1), 108–116.
 Kurian, M.A., Gissen, P., Smith, M., Heales, S.J.R., Clayton, P.T., 2011. Lancet Neurol. 10 (8), 721–733.
- Lin, Y.Q., Yu, P., Hao, J., Wang, Y.X., Ohsaka, T., Mao, L.Q., 2014. Anal. Chem. 86 (8), 3895–3901.
- Liu, C.B., Zhao, Y., Cai, X., Xie, Y., Wang, T.Y., Cheng, D.L., Li, L.Z., Li, R.F., Deng, Y.P., Ding, H., Lv, G.Q., Zhao, G.L., Liu, L., Zou, G.S., Feng, M.X., Sun, Q.A., Yin, L., Sheng, X., 2020. Microsyst Nanoeng 6 (1).
- Maenner, M.J., Shaw, K.A., Bakian, A.V., Bilder, D.A., Durkin, M.S., Esler, A., Furnier, S.
 M., Hallas, L., Hall-Lande, J., Hudson, A., Hughes, M.M., Patrick, M., Pierce, K.,
 Poynter, J.N., Salinas, A., Shenouda, J., Vehorn, A., Warren, Z., Constantino, J.N.,
 DiRienzo, M., Fitzgerald, R.T., Grzybowski, A., Spivey, M.H., Pettygrove, S.,
 Zahorodny, W., Ali, A., Andrews, J.G., Baroud, T., Gutierrez, J., Hewitt, A., Lee, L.C.,
 Lopez, M., Mancilla, K.C., McArthur, D., Schwenk, Y.D., Washington, A.,
 Williams, S., Cogswell, M.E., 2021. Mmwr Surveill Summ 70 (11).
- Manyukhina, V.O., Prokofyev, A.O., Galuta, I.A., Goiaeva, D.E., Obukhova, T.S., Schneiderman, J.F., Altukhov, D.I., Stroganova, T.A., Orekhova, E.V., 2022. Mol. Autism. 13 (1).
- Moldovan, N., Blaga II, Billa, S., Hossain, I., Gong, C., Jones, C.E., Murray, T.A., Divan, R., Siddiqui, S., Arumugam, P.U., 2021. Sensor. Actuator. B Chem. 337.
- Moreira, F.T.C., Sale, M.G.F., Di Lorenzo, M., 2017. Biosens. Bioelectron. 87, 607–614.
 Ou, Y.G., Buchanan, A.M., Witt, C.E., Hashemi, P., 2019. Anal Methods-Uk 11 (21), 2738–2755.
- Reinhoud, N.J., Brouwer, H.J., van Heerwaarden, L.M., Korte-Bouws, G.A.H., 2013. ACS Chem. Neurosci. 4 (5), 888–894.
- Rezaei, B., Irannejad, N., 2019. Electrochemical Biosensors. Elsevier, pp. 11–43.
 Robinson, D.L., Hermans, A., Seipel, A.T., Wightman, R.M., 2008. Chem. Rev. 108 (7), 2554–2584.
- Sandberg, S.G., Garris, P.A., 2010. Advances in the Neuroscience of Addiction, pp. 99–135.
- Saylor, R.A., Thomas, S.R., Lunte, S.M., 2017. COMPENDIUM OF IN VIVO MONITORING IN REAL-TIME MOLECULAR NEUROSCIENCE, vol. 2. Microdialysis and Sensing of Neural Tissues, pp. 1–45.
- Serio, A., Bilican, B., Barmada, S.J., Ando, D.M., Zhao, C., Siller, R., Burr, K., Haghi, G., Story, D., Nishimura, A.L., Carrasco, M.A., Phatnani, H.P., Shum, C., Wilmut, I., Maniatis, T., Shaw, C.E., Finkbeiner, S., Chandran, S., 2013. P Natl Acad Sci USA 110 (12), 4697–4702.
- Wahono, N., Qin, S., Oomen, P., Cremers, T.I.F., de Vries, M.G., Westerink, B.H.C., 2012. Biosens. Bioelectron. 33 (1), 260–266.
- Weltin, A., Kieninger, J., Urban, G.A., 2016. Anal. Bioanal. Chem. 408 (17), 4503–4521.
 Wen, X.M., Wang, B., Huang, S., Liu, T.Y., Lee, M.S., Chung, P.S., Chow, Y.T., Huang, I. W., Monbouquette, H.G., Maidment, N.T., Chiou, P.Y., 2019. Biosens. Bioelectron. 131, 37–45.
- Zaib, M., Athar, M.M., 2018. Instrum. Sci. Technol. 46 (4), 408–425.
- Zhao, H.S., Mao, X.J., Zhu, C.L., Zou, X.H., Peng, F.Z., Yang, W., Li, B.J., Li, G.Q., Ge, T. T., Cui, R.J., 2022. Front. Cell Dev. Biol. 9
- Zhou, D.M., Dai, Y.Q., Shiu, K.K., 2010. J. Appl. Electrochem. 40 (11), 1997–2003.